Chemical Engineering Journal 147 (2009) 202–209

Contents lists available at ScienceDirect

Chemical Engineering Journal

journal homepage: www.elsevier.com/locate/cej

Exponential model analysis of permeate flux for ultrafiltration in hollow-fiber modules by momentum balance

H.M. Yeh*

Department of Chemical and Materials Engineering, Tamkang University, Tamsui 251, Taiwan

ARTICLE INFO

Article history:
Received 9 October 2007
Received in revised form 20 June 2008
Accepted 1 July 2008

Keywords:
Ultrafiltration
Exponential model
Momentum balance

ABSTRACT

The modified correlation equation for predicting the permeate flux of membrane ultrafiltration (UF) in hollow-fiber modules was derived from the complete momentum balance coupled with the application of exponential model. The correlation predictions obtained in present study are more accurate than those obtained in the previous works, in which the momentum balance was taken inaccurately by simply applying Hagen–Poiseuille theory without the consideration of the effect of permeate flux loss, as well as the effect of the loss of momentum transfer due to convection, on overall momentum balance.

1. Introduction

Ultrafiltration (UF) is a pressure-driven membrane separation process. The working pressure, usually applied to the solution in the range of 100–1000 kPa, provides the driving potential to force the solvent or the solute consisting of smaller molecules to flow through the membrane while the larger molecules are rejected by the membrane. Therefore, the main application of UF is the separation of fairly large molecules. Nowadays, it is applied in a wide variety of fields, from the chemical industry (including eletrocoat paint recovery, latex processing, textile size recovery and recovery of lubricating oil), to medical applications (such as kidney dialysis operation), and even to biotechnology (including concentration of milk, egg white, juice, pectin and sugar, and recovery of protein from cheese whey, animal blood, gelatin and glue) [1–3].

Membrane UF process is usually analyzed by the gel polarization model [4–10], the osmotic pressure model [11–19], and the resistance-in-series model [20–22]. In the gel polarization model, permeate flux is reduced by the hydraulic resistance of gel layer. In the osmotic pressure model, permeate flux reduction results from the decrease in effective transmembrane pressure that occurs as the osmotic pressure of the retentate increases. In the resistance-in-series model, permeate flux decreases due to the resistances caused by fouling or solute adsorption and concentration polarization (CP). Recently, new theoretical modeling has been carried out in detail at the University of Bath, UK [23,24]. Further, Song and Elimelech [25] developed the fundamental theory and methodology providing a solid basis for the study of limiting flux in UF. Later, a mechanistic model for predicting the limiting flux in UF was also developed [26]. In this study, the exponential model for predicting the permeate flux of UF in hollow-fiber modules is introduced, and the incline of transmembrane pressure due to the momentum loss by convection is taken into consideration.

2. Theory

Consider a hollow-fiber module with N fibers of same size, in which the membrane is formed on the inside of N tiny porous tubes that are then bundled and potted into a tube-and-shell arrangement, as shown in Fig. 1, while Fig. 2 shows the flows and fluxes in the fiber tube of radius r_m and length L.

2.1. Mass balance

Let $q(z)N$ be the volumetric flow rate of solution in a hollow fiber and J be the permeate flux by ultrafiltration. Then, a mass balance over a slice dz of the fiber gives

$$\frac{d(q/N)}{dz} = -2\pi r_m J \quad (1)$$

2.2. Momentum balance

The problem dealing with the pressure distribution can be approached by setting up momentum balance within the differ-

* Tel.: +886 2 2621 5656x2601; fax: +886 2 2620 9887.
E-mail address: hmyeh@mail.tku.edu.tw.

1385-8947/$ – see front matter © 2008 Elsevier B.V. All rights reserved.
doi:10.1016/j.cej.2008.07.002

Nomenclature

C_i	concentration of feed solution (wt%)
J	permeate flux of solution ($m^3/(m^2\,s)$)
J_{lim}	limiting flux ($m^3/(m^2\,s)$)
L	effective length of hollow fiber (m)
N	number of hollow fibers in a membrane module
p	pressure distribution on the tube side (Pa)
p_s	uniform permeate pressure on the shell side (Pa)
Δp	transmembrane pressure, $p - p_s$ (Pa)
ΔP	dimensionless transmembrane pressure, $\Delta p/\Delta p_i$
q	volume flow rate in a hollow-fiber module (m^3/s)
Q	dimensionless flow rate, defined by Eq. (10)
r_m	inside radius of hollow fiber (m)
R	total resistances (Pa s/m)
u	fluid velocity in the hollow fiber, $q/N(\pi r_m^2)$ (m/s)
V	dimensionless permeate flux, defined by Eq. (7)
z	axial coordinate (m)
Z	dimensionless axial coordinate, z/L

Greek letters

α	dimensionless group, defined by Eq. (11)
β	dimensionless group, defined by Eq. (8)
γ	dimensionless group, defined by Eq. (12)
μ	viscosity of solution (Pa s)

Subscripts

i	at the inlet
o	at the outlet
exp	experimental value

Superscript

–	average value

ential length dz of a hollow fiber. For steady-state operation [27]

$$\frac{d}{dz}(\rho u_b^2) + \frac{d}{dz}(\Delta p) + \frac{\tau_s(2\pi r_m)}{\pi r_m^2} = 0 \tag{2}$$

where Δp ($=p - p_s$) denotes the transmembrane pressure, and $p(z)$ and p_s are the pressures in fiber tube and shell sides, respectively, while the shear stress τ_s relates to the friction factor f and bulk velocity of fluid u_b as $\tau_s = (\rho u_b^2/2)f$. For laminar flow, $f = 16/(2r_m u_b \rho/\mu)$, and for flow in a tube, $(q/N) = \pi r_m^2 u_b$, the above equation can be rewritten as:

$$\frac{\rho}{\pi^2 r_m^4}\frac{d(q/N)^2}{dz} + \frac{d\Delta p}{dz} + \frac{8\mu(q/N)}{\pi r_m^4} = 0 \tag{3}$$

The three terms on the left-hand side of Eq. (3) denote, respectively, the rate of momentum transfer by convection, the pressure force and the rate of momentum by viscous transfer.

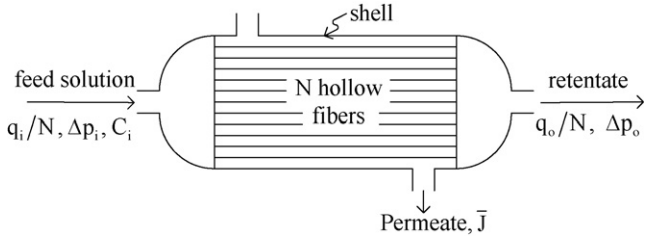

Fig. 1. Hollow-fiber ultrafilter.

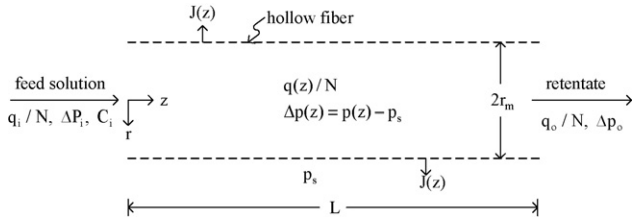

Fig. 2. Flows and fluxes in a hollow fiber for ultrafiltration.

2.3. Exponential model

As mentioned before, membrane ultrafiltration is a pressure-driven process, and permeate flux is a power function of applied pressure. However, as the pressure continuously increases, the limiting flux, J_{lim}, is reached where any further pressure increase no longer results in any increase in flux. Accordingly, the following relations between permeate flux $J(z)$ and transmembrane pressure Δp are reached:

$$J = 0, \quad \text{for } \Delta P = 0 \tag{4}$$

$$J = J_{lim}, \quad \text{as } \Delta P \to \infty \text{(or large enough)} \tag{5}$$

Therefore, the exponential model is thus introduced and may be expressed as

$$V = 1 - e^{-\beta\,\Delta P} \tag{6}$$

in which

$$V = \frac{J}{J_{lim}} \tag{7}$$

$$\Delta P = \frac{\Delta p}{\Delta p_i} \tag{8}$$

$$\beta = \frac{\Delta p_i}{R J_{lim}} \tag{9}$$

where Δp_i is the transmembrane pressure at the inlet and R denotes the total resistances of ultrafiltration due to the intrinsic resistance, concentration polarization and fouling. J_{lim} and R can be determined experimentally. It is easy to check that Eq. (6) satisfies Eqs. (4) and (5).

2.4. Decline of transmembrane pressure

Define the following dimensionless groups with fiber length L:

$$Q = \frac{8\mu L(q/N)}{\pi r_m^4\,\Delta p_i} \tag{10}$$

$$\alpha = \frac{16\mu L^2 J_{lim}}{r_m^3(\Delta p_i)} \tag{11}$$

$$\gamma = \frac{\rho r_m^4(\Delta p_i)}{64\mu^2 L^2} \tag{12}$$

$$Z = \frac{z}{L} \tag{13}$$

With the use of above relations, Eqs. (1) and (3) may be rewritten as

$$\frac{dQ}{dZ} = -\alpha V \tag{14}$$

$$\gamma\frac{dQ^2}{dZ} + \frac{d\Delta P}{dZ} + Q = 0 \tag{15}$$

Substitution of Eq. (6) into Eq. (14) yields

$$\frac{dQ}{dZ} = -\alpha(1 - e^{-\beta\ \Delta P}) \tag{16}$$

The flow rate of solution declines along the fiber tube due to membrane ultrafiltration and thus, solvent is permeated through the porous tube wall by transmembrane pressure. For mathematical simplicity, we may assume that q/N declines linearly along the hollow fiber by approximately setting $\Delta p = \Delta p_i$ ($\Delta P = 1$) in Eq. (16). Accordingly, integration of Eq. (16) from $Z = 0$ ($Q = Q_i$, i.e., $q = q_i$) to $Z = Z$ results in

$$Q = Q_i - \alpha \int_0^Z (1 - e^{-\beta})\ dZ = Q_i - \alpha(1 - e^{-\beta})Z \tag{17}$$

Substituting Eq. (17) into Eq. (15) and integrating from $Z = 0$ ($\Delta P = 1$) to Z, one obtains

$$\Delta P = 1 - [1 - 2\alpha\gamma(1 - e^{-\beta})]\left[Q_i Z - \left(\frac{\alpha}{2}\right)(1 - e^{-\beta})\ Z^2\right] \tag{18}$$

or

$$\Delta P = 1 + \left(\frac{\alpha}{2}\right)(1 - e^{-\beta})[1 - 2\alpha\gamma(1 - e^{-\beta})] \times \left[Z^2 - 2\left\{\frac{Q_i}{\alpha(1 - e^{-\beta})}\right\}Z\right] \tag{19}$$

Once ΔP is calculated from above equations, the declining fluxes, J and V ($= J/J_{lim}$), are readily obtained from Eq. (6).

2.5. Average permeate flux

The average permeate flux can be obtained from

$$\bar{J} = \frac{1}{L}\int_0^L J(z)\ dz \tag{20}$$

or, in dimensionless form

$$\bar{V} = \int_0^1 V(Z)\ dZ \tag{21}$$

where

$$\bar{V} = \frac{\bar{J}}{J_{lim}} \tag{22}$$

Substituting Eqs. (6) and (19) into Eq. (21), we have

$$\bar{V} = 1 - e^{-\beta}\int_0^1 e^{-A^2[Z^2 - 2BZ]}\,dZ = 1 - \left(\frac{1}{A}\right)e^{(A^2B^2 - \beta)}\int_{-AB}^{A(1-B)} e^{-A^2(Z-B)^2}\,d[A(Z - B)] \tag{23}$$

where

$$A = \left\{\left(\frac{\alpha\beta}{2}\right)(1 - e^{-\beta})[1 - \alpha\gamma(1 - e^{-\beta})]\right\}^{1/2} \tag{24}$$

$$B = \frac{Q_i}{\alpha(1 - e^{-\beta})} \tag{25}$$

The error function is defined as

$$\text{erf}\ \eta = \frac{2}{\sqrt{\pi}}\int_0^\eta e^{-\xi^2}d\xi \tag{26}$$

and

$$\frac{2}{\sqrt{\pi}}\int_{-\eta_1}^{\eta_2} e^{-\xi^2}d\xi = \text{erf}\,\eta_2 - \text{erf}(-\eta_1) = \text{erf}\,\eta_2 + \text{erf}\,\eta_1 \tag{27}$$

Accordingly, Eq. (23) may be rewritten in terms of error functions as

$$\bar{V} = 1 - \left(\frac{\sqrt{\pi}}{2A}\right)[\exp(A^2B^2 - \beta)][\text{erf}\{A(1 - B)\} + \text{erf}(AB)] \tag{28}$$

3. Results and discussion

3.1. Previous works

The theoretical predictions of average permeate flux $\bar{J}$ will be compared with those obtained in the previous works [22,28,29], in which the rate of momentum transfer by convection along the fiber tube was neglected, i.e., $\gamma = 0$ in Eq. (15). An Amicon model H1P 30-20 hollow-fiber cartridge ($r_m = 2.5 \times 10^{-4}$ m, $L = 0.153$ m, $N = 250$, MWCO = 30,000) made of polysulfone were used for experimental studies of the membrane ultrafiltration of aqueous solutions of dextran T500 (Pharmacia Co., $M_n = 170{,}300$) [22], polyvinylpyrrolidone (PVP-360, Sigma Co., $M_n = 360{,}000$) [28] and polyvinyl alcohol (PVA, Sigma Co., $M_n = 320{,}000$) [29]. The experimental results for these three aqueous solutions are presented in Tables 1–3, respectively, while some of the corresponding average permeate fluxes are shown in Figs. 3 and 4, Figs. 5 and 6 and Figs. 7 and 8.

3.2. Determination of J_{lim} and R

It was found from the experimental values of $\bar{J}_{exp}$ and $(\overline{\Delta P})_{exp}$ that $(1/\bar{J})_{exp}$ vs. $(1/\overline{\Delta p})_{exp}$ is a straight line [20,31,32]. Accordingly, when the abscissa $(1/\overline{\Delta p})_{exp}$ is zero, i.e., $(\overline{\Delta p})_{exp} \to \infty$, the intersection of the straight line at the ordinate will be $(1/J_{lim})$, as indicated by Eq. (5). Further, Eq. (6) may be rewritten as

$$1 - \left(\frac{\bar{J}}{J_{lim}}\right)_{exp} = e^{-(\overline{\Delta p})_{exp}/(RJ_{lim})} \tag{29}$$

Consequently, the straight-line plot of $-\ln(1 - \bar{J}/J_{lim})_{exp}$ vs. $(\overline{\Delta p})_{exp}$ will result in the slope of $1/(RJ_{lim})$. Some experimental values of J_{lim} and $1/(RJ_{lim})$, as well as the resistance of ultrafiltration, R, for dextran T500, PVP 360 and PVA systems are listed in Tables 4–6, respectively.

The correlation equations of J_{lim} and R were then obtained by the method of least squares [28–31] with the use of the experimental data in Tables 4–6. They are

$$J_{lim}(m/s) = 4.022 \times 10^{-5} u_i^{1.266} C_i^{-1.783} \tag{30}$$

$$R(Pa\,s/m) = 1.382 \times 10^{9} u_i^{-1.14} C_i^{1.766} \tag{31}$$

$$\mu(Pa\,s) = 0.894 \times 10^{-3}\ \exp(0.408 C_i) \tag{32}$$

for dextran 500 system,

$$J_{lim}(m/s) = 2.524 \times 10^{-5} u_i^{0.765} C_i^{-0.3} \tag{33}$$

$$R(Pa\,s/m) = 7.2 \times 10^{9} u_i^{-0.38} C_i^{0.227} \tag{34}$$

$$\mu(Pa\,s) = 0.894 \times 10^{-3}\ \exp(0.875 C_i) \tag{35}$$

for PVP 360 system, and

$$J_{lim}(m/s) = 1.11 \times 10^{-4} u_i^{2.44} C_i^{-0.309} \tag{36}$$

$$R(Pa\,s/m) = 5.64 \times 10^{9} u_i^{-0.57} C_i^{0.26} \tag{37}$$

$$\mu(Pa\,s) = 3.2 \times 10^{-3} \tag{38}$$

for PVA aqueous solution. It is noted that for the use of calculating the permeate flux, the correlation equations of viscosity, μ, are

Table 1
Experimental data of dextran T500 aqueous solution [22]

C_i (wt%)	Δp_i ($\times 10^{-5}$ Pa)	u_i = 0.051 m/s		u_i = 0.102 m/s		u_i = 0.204 m/s		u_i = 0.306 m/s	
		$\overline{\Delta p}$ ($\times 10^{-5}$ Pa)	$\bar{J}$ ($\times 10^{6}$ m^3/(m^2 s))	$\overline{\Delta p}$ ($\times 10^{-5}$ Pa)	$\bar{J}$ ($\times 10^{6}$ m^3/(m^2 s))	$\overline{\Delta p}$ ($\times 10^{-5}$ Pa)	$\bar{J}$ ($\times 10^{6}$ m^3/(m^2 s))	$\overline{\Delta p}$ ($\times 10^{-5}$ Pa)	$\bar{J}$ ($\times 10^{6}$ m^3/(m^2 s))
0.1	0.3	0.251	3.4	0.241	3.82	0.225	4.02	0.204	3.98
	0.5	0.451	4.25	0.443	4.88	0.426	5.53	0.406	5.93
	0.7	0.651	4.78	0.643	5.61	0.627	6.44	0.605	6.95
	1.0	0.951	5.37	0.942	6.24	0.925	7.27	0.906	8.17
	1.4	1.350	5.83	1.338	6.76	1.323	7.99	1.303	9.08
0.2	0.3	0.252	2.70	0.240	3.08	0.225	3.40	0.198	3.35
	0.5	0.452	3.21	0.442	3.84	0.424	4.44	0.400	4.86
	0.7	0.652	3.54	0.642	4.30	0.622	4.96	0.601	5.62
	1.0	0.952	3.82	0.942	4.67	0.924	5.52	0.903	6.36
	1.4	1.351	4.20	1.340	5.09	1.321	6.07	1.303	7.02
0.5	0.3	0.245	2.02	0.235	2.29	0.213	2.55	0.185	2.64
	0.5	0.446	2.34	0.433	2.73	0.413	3.28	0.388	3.64
	0.7	0.647	2.50	0.634	2.99	0.615	3.62	0.585	4.14
	1.0	0.945	2.67	0.936	3.21	0.912	3.98	0.886	4.57
	1.4	1.339	2.86	1.340	3.46	1.317	4.28	1.287	5.00
1.0	0.3	0.243	1.54	0.228	1.73	0.200	1.92	0.165	1.85
	0.5	0.445	1.79	0.429	2.07	0.400	2.50	0.365	2.64
	0.7	0.642	1.93	0.629	2.29	0.600	2.78	0.564	3.03
	1.0	0.942	2.06	0.930	2.46	0.901	3.05	0.864	3.36
	1.4	1.337	2.18	1.330	2.62	1.299	3.24	1.264	3.62
2.0	0.3	0.236	1.09	0.211	1.21	0.165	1.26	0.216	1.60
	0.5	0.435	1.30	0.410	1.52	0.363	1.81	0.316	1.94
	0.7	0.635	1.43	0.611	1.69	0.563	2.06	0.513	2.34
	1.0	0.935	1.56	0.911	1.84	0.862	2.29	0.813	2.68
	1.4	1.327	1.66	1.311	1.96	1.260	2.49	1.214	2.92

Table 2
Experimental data of PVP 360 aqueous solution [28]

C_i (wt%)	Δp_i ($\times 10^{-5}$ Pa)	u_i = 0.0723 m/s		u_i = 0.1209 m/s		u_i = 0.1684 m/s		u_i = 0.2195 m/s	
		$\overline{\Delta p}$ ($\times 10^{-5}$ Pa)	$\bar{J}$ ($\times 10^6$ m^3/(m^2 s))	$\overline{\Delta p}$ ($\times 10^{-5}$ Pa)	$\bar{J}$ ($\times 10^6$ m^3/(m^2 s))	$\overline{\Delta p}$ ($\times 10^{-5}$ Pa)	$\bar{J}$ ($\times 10^6$ m^3/(m^2 s))	$\overline{\Delta p}$ ($\times 10^{-5}$ Pa)	$\bar{J}$ ($\times 10^6$ m^3/(m^2 s))
0.1	1.15	1.065	6.3	1.05	8.35	1.04	10.01	1.045	11.38
	0.96	0.87	5.96	0.85	7.81	0.845	9.57	0.86	10.71
	0.77	0.68	5.78	0.66	7.54	0.665	9.00	0.66	9.89
	0.57	0.49	5.43	0.48	6.73	0.475	7.82	–	–
	0.38	0.295	4.54	–	–	–	–	–	–
0.5	1.15	1.065	3.56	1.05	4.97	1.04	6.21	1.04	7.38
	0.96	0.87	3.47	0.86	4.96	0.845	6.07	0.845	7.18
	0.77	0.68	3.43	0.67	4.76	0.655	5.88	0.655	6.83
	0.57	0.49	3.22	0.48	4.44	0.465	5.42	0.465	6.08
	0.38	0.295	2.78	0.29	3.68	0.285	4.21	0.275	4.73
	0.19	0.11	1.93	–	–	–	–	–	–
1.0	1.15	1.045	2.79	1.045	4.23	1.025	5.23	1.01	6.21
	0.96	0.85	2.77	0.85	4.18	0.835	5.10	0.82	5.93
	0.77	0.66	2.70	0.66	4.04	0.645	4.92	0.63	5.75
	0.57	0.475	2.52	0.475	3.72	0.455	4.38	0.44	5.19
	0.38	0.29	2.22	0.285	3.09	0.265	3.44	0.255	3.78
	0.19	0.1	1.47	–	–	–	–	–	–

Table 3
Experimental data of PVA aqueous solution [29]

C_i (wt%)	Δp_i ($\times 10^{-5}$ Pa)	u_i = 0.0625 m/s		u_i = 0.1042 m/s		u_i = 0.1458 m/s		u_i = 0.1875 m/s	
		$\overline{\Delta p}$ ($\times 10^{-5}$ Pa)	$\bar{J}$ ($\times 10^6$ m^3/(m^2 s))	$\overline{\Delta p}$ ($\times 10^{-5}$ Pa)	$\bar{J}$ ($\times 10^6$ m^3/(m^2 s))	$\overline{\Delta p}$ ($\times 10^{-5}$ Pa)	$\bar{J}$ ($\times 10^6$ m^3/(m^2 s))	$\overline{\Delta p}$ ($\times 10^{-5}$ Pa)	$\bar{J}$ ($\times 10^6$ m^3/(m^2 s))
0.01	0.3	0.2695	0.488	0.2695	1.584	0.245	3.168	0.2205	4.883
	0.5	0.466	0.503	0.466	1.688	0.4415	3.582	0.417	6.005
	0.7	0.662	0.510	0.662	1.734	0.6375	3.766	0.613	6.517
	0.9	0.883	0.512	0.883	1.759	0.8335	3.869	0.809	6.811
0.05	0.3	0.2695	0.307	0.2695	1.023	0.245	2.130	0.2205	3.452
	0.5	0.466	0.313	0.466	1.097	0.4415	2.327	0.417	4.026
	0.7	0.662	0.316	0.662	1.089	0.6375	2.409	0.613	4.267
	0.9	0.883	0.317	0.883	1.100	0.8335	2.454	0.809	4.399
0.1	0.3	0.2695	0.249	0.2695	0.838	0.245	1.761	0.2205	2.889
	0.5	0.466	0.255	0.466	0.873	0.4415	1.910	0.417	3.332
	0.7	0.662	0.257	0.662	0.888	0.6375	1.971	0.613	3.512
	0.9	0.883	0.258	0.883	0.896	0.8335	2.004	0.809	3.610
0.5	0.3	0.2695	0.147	0.245	0.460	0.2205	0.849	0.196	1.007
	0.5	0.466	0.153	0.4415	0.511	0.427	1.078	0.3925	1.789
	0.7	0.662	0.155	0.6275	0.529	0.613	1.153	0.5885	2.008
	0.9	0.883	0.157	0.8335	0.523	0.809	1.190	0.7845	2.114

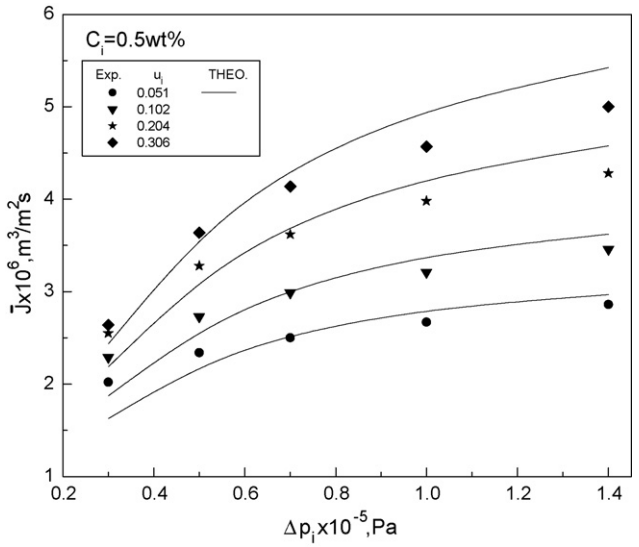

Fig. 3. Comparison of the predicting values with the experimental results for average permeate flux of dextran T500 system for C_i = 0.5 wt%.

also provided in Eqs. (32), (35) and (38) [31,32]. The average value of viscosity ($\mu = 3.2 \times 10^{-3}$ Pa s) for PVA system was measured at 25 °C for C_i = 0.01–0.5 wt%.

3.3. Correlation predictions

The correlation predictions of average permeate flux, $\bar{J}$, under various inlet transmembrane pressures, Δp_i, feed concentrations, C_i and fluid velocities, u_i, were calculated from Eqs. (22) and (28) coupled with the use of Eqs. (30)–(38). The calculated results are plotted and compared with the experimental data, as shown in Figs. 3–8. It is seen in these figures that the correlation predictions for PVA aqueous solution are better in agreement with the experimental results than those for the aqueous solutions of dextran T500 and PVP 360. Nevertheless, the deviations of theoretical predictions from the experimen-

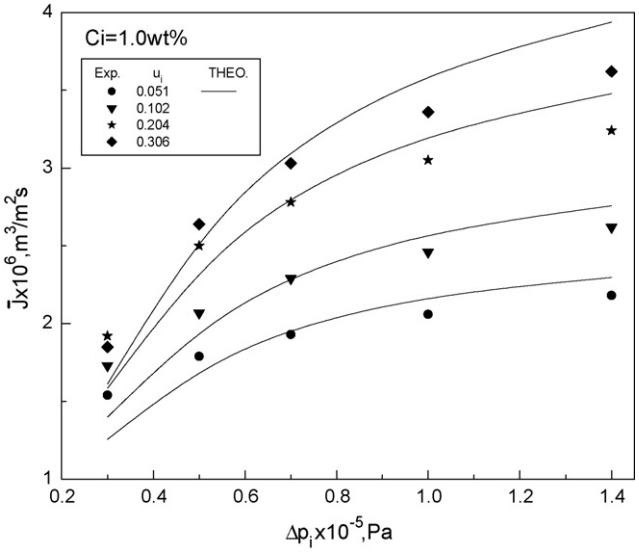

Fig. 4. Comparison of the predicting values with the experimental results for average permeate flux of dextran T500 system for C_i = 1.0 wt%.

Table 4
The fitting parameters of experimental data for dextran T500 aqueous solution

C_i (wt%)	u_i (m/s)	J_{lim} ($\times 10^5$ m^3/(m^2 s))	$(RJ_{lim})^{-1}$ ($\times 10^5$ Pa^{-1})	R ($\times 10^{-9}$ Pa s/m)
0.1	0.051	5.64	2.50	0.71
	0.102	13.56	2.30	0.32
	0.204	32.61	2.14	0.14
	0.306	54.49	2.04	0.09
0.2	0.051	1.60	2.60	2.40
	0.102	3.94	2.33	1.09
	0.204	9.48	2.15	0.49
	0.306	15.83	2.04	0.31
0.5	0.051	0.31	2.67	12.08
	0.102	0.77	2.37	5.48
	0.204	1.85	2.17	2.49
	0.306	3.09	2.06	1.57
1.0	0.051	0.09	2.70	41.10
	0.102	0.22	2.44	18.65
	0.204	0.54	2.19	8.46
	0.306	0.90	2.08	5.33
2.0	0.051	0.027	2.65	139.75
	0.102	0.065	2.43	63.41
	0.204	0.156	2.23	28.76
	0.306	0.260	2.12	18.12

Table 5
The fitting parameters of experimental data for PVP 360 aqueous solution

C_i (wt%)	u_i (m/s)	J_{lim} ($\times 10^6$ m^3/(m^2 s))	$(RJ_{lim})^{-1}$ ($\times 10^5$ Pa^{-1})	R ($\times 10^{-9}$ Pa s/m)
0.1	0.0723	7.30	1.29	10.62
	0.1209	10.25	1.02	9.56
	0.1684	13.24	0.91	8.30
	0.2195	15.26	0.85	7.71
0.5	0.0723	3.95	1.68	15.07
	0.1209	5.94	1.11	15.17
	0.1684	7.85	1.06	12.02
	0.2195	9.51	1.05	10.01
1.0	0.0723	3.18	1.56	20.16
	0.1209	5.19	1.53	12.59
	0.1684	6.52	1.13	13.57
	0.2195	8.20	0.99	12.32

Table 6
The fitting parameters of experimental data for PVA aqueous solution

C_i (wt%)	u_i (m/s)	J_{lim} ($\times 10^6$ m^3/(m^2 s))	$(RJ_{lim})^{-1}$ ($\times 10^5$ Pa^{-1})	R ($\times 10^{-9}$ Pa s/m)
0.01	0.0625	0.52	21.85	8.80
	0.1042	1.83	8.19	6.67
	0.1458	4.18	4.28	5.59
	0.1875	7.74	2.62	4.94
0.05	0.0625	0.32	31.57	9.90
	0.1042	1.13	11.74	7.54
	0.1458	2.59	6.12	6.31
	0.1875	4.82	3.70	5.60
0.1	0.0625	0.26	34.46	11.13
	0.1042	0.91	13.34	8.24
	0.1458	2.08	7.13	6.74
	0.1875	3.80	4.55	5.78
0.5	0.0625	0.16	27.33	32.87
	0.1042	0.56	10.45	17.09
	0.1458	1.24	3.78	16.90
	0.1875	2.23	3.67	12.23

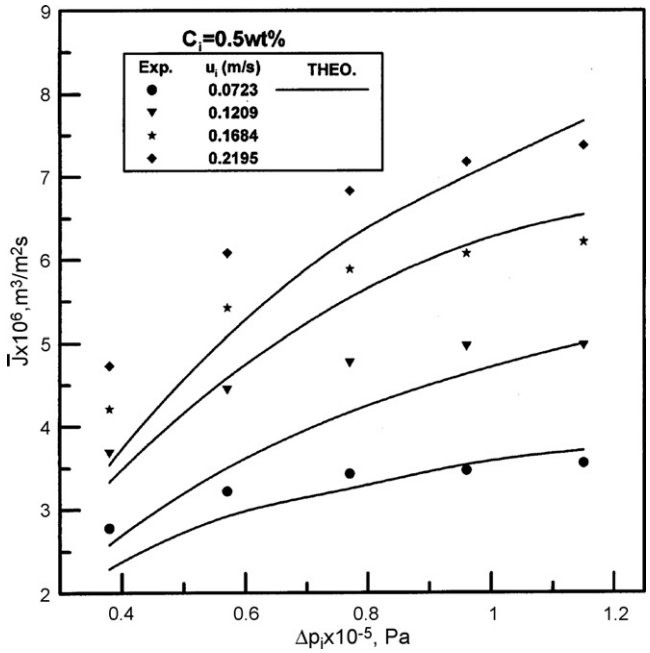

Fig. 5. Comparison of the predicting values with the experimental results for average permeate flux of PVP 360 system for C_i = 0.5wt%.

tal results are small for dextran T500 system within the middle range of transmembrane pressures ($\Delta P_i = 0.4 \times 10^5 - 0.8 \times 10^5$ Pa) and for PVP 360 system under rather higher transmembrane pressures ($\Delta P_i = 0.7 \times 10^5 - 1.0 \times 10^5$ Pa). As a while, the deviation turns smaller as the fluid velocity decreases. It is concluded that the exponential model is more suitable for the permeation analysis of ultrafiltration of polyvinyl alcohol aqueous solution in a hollow-fiber cartridge.

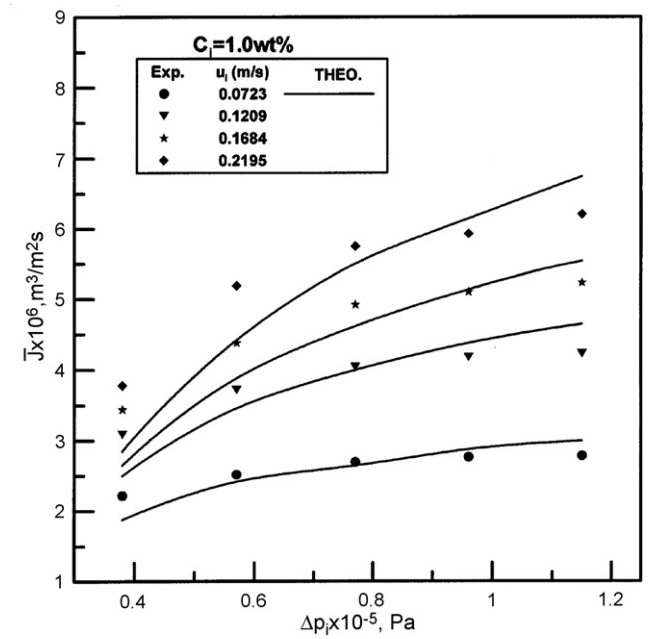

Fig. 6. Comparison of the predicting values with the experimental results for average permeate flux of PVP 360 system for C_i = 1.0 wt%.

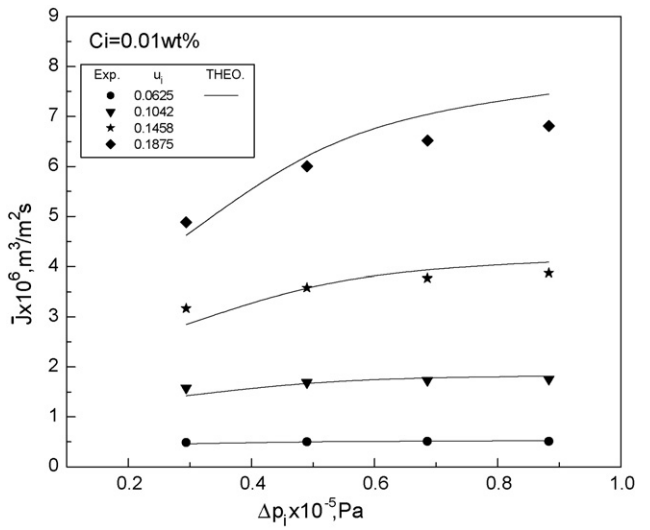

Fig. 7. Comparison of the predicting values with the experimental results for average permeate flux of PVA system for C_i = 0.01 wt%.

3.4. Confirmation of the assumptions made

The assumption of laminar flow is easy to check by the maximum value of Reynolds number for PVA 360 system with u_i = 0.2195 m/s, C_i = 0.1 wt%, and $\bar{J} = 11.38 \times 10^{-6}$ m^3/m^2 s as

$$(Re)_{max} = \frac{2r_m u_i \rho}{\mu} = \frac{2(2.5 \times 10^{-4})(0.2195)(1000)}{0.8937 \times 10^{-3}\ e^{0.875(0.1)}} = 112.5 < 2100$$

Therefore, the assumption of laminar flow is acceptable for the system of present interest. Further since

$$\frac{q_i}{N} = \pi r_m^2 u_i = \pi(2.5 \times 10^{-4})^2(0.2195) = 4.31 \times 10^{-8}\ \text{m}^3/\text{s}$$

$$2\pi r_m L\bar{J} = 2\pi(2.5 \times 10^{-4})(0.153)(11.38 \times 10^{-6}) = 2.73 \times 10^{-9}\ \text{m}^3/\text{s}$$

and

$$\frac{q_o}{N} = \frac{q_i}{N} - 2\pi r_m L\bar{J} = 4.04 \times 10^{-8}\ \text{m}^3/\text{s}$$

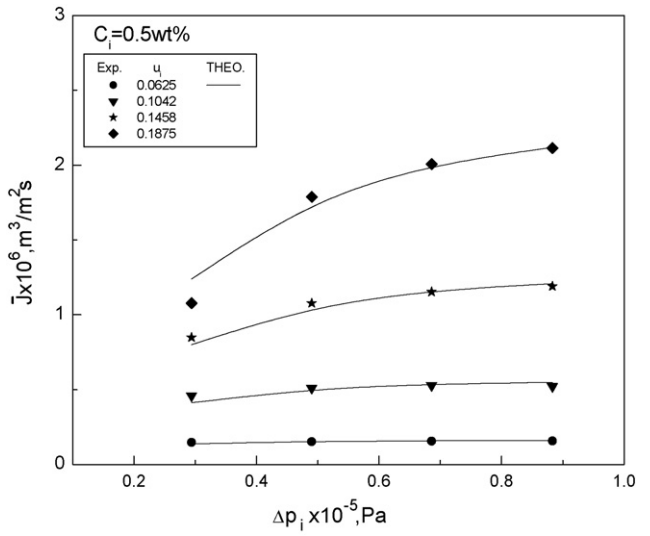

Fig. 8. Comparison of the predicting values with the experimental results for average permeate flux of PVA system for C_i = 0.5 wt%.

Consequently, the assumption that q/N declines linearly is acceptable.

4. Conclusion

The predicting equation, Eq. (28), for the average permeate fluxes of membrane ultrafiltration in hollow-fiber modules, was derived by the exponential model coupled with the application of complete momentum balance, in which the momentum transfer by convection (fluid motion) was taken into consideration. It is found that the correlation predictions of permeate flux obtained in present study are more accurate than those obtained in the previous works [22,28,29], in which the momentum balance was taken inaccurately by simply applying Hagen–Poiseuille theory without the considerations of the effects of permeate flux loss and the loss of momentum flux due to fluid motion, on overall momentum balance.

As mentioned earlier, the exponential model satisfies the two essential conditions of membrane ultrafiltration, Eqs. (4) and (5). Further, the mathematical treatment for deriving the predicting equation of permeate flux is easier than other models, even with the consideration of the momentum transfer by convection. Therefore, the present model easily describes the relationships of permeate flux with operating and design parameters, and we believe that this model will also be suitable for most membrane ultrafiltration systems including systems with different kinds of feed solutions, different materials of membrane tubes, and various design and operating conditions.

Acknowledgement

The authors wish to express their thanks to the National Science Council of ROC for financial aid with the Grant No. NSC 94-2214-E-02-005.

References

[1] S.S. Kulkarni, E.W. Funk, N.N. Li, Ultrafiltration, in: W.S.W. Ho, K.K. Sirkar (Eds.), Membrane Handbook, Chapman and Hall, New York, 1992, p. 393.
[2] M.C. Porter, Membrane filtration, in: P.A. Schweitzer (Ed.), Handbook of Separation Techniques for Chemical Engineers, McGraw-Hill, New York, 1979, (Section 2.1).
[3] M. Cheryan, Ultrafiltration, Handbook, Technomic Publishing Co., Inc., Lancaster/Pennsylvania, 1986 (Section 8).
[4] S. Nokao, T. Nomura, S. Kimura, Characteristics of macromolecular gel layer formed on ultrafiltration tubular membrane, AIChE J. 25 (1979) 615.
[5] A.G. Fane, C.J.D. Fell, A.G. Waters, The relationship between membrane surface pore characteristics and flux for ultrafiltration membranes, J. Member. Sci. 9 (1981) 245.
[6] W.F. Blatt, A. Dravid, A.S. Michales, L. Nelsen, Solute polarization and cake formation in membrane ultrafiltration: causes, consequences, and control techniques, in: J.E. Filnn (Ed.), Membrane Science and Technology, Plenum Press, New York, 1970, p. 47.
[7] M.C. Porter, Concentration polarization with membrane ultrafiltration, Ind. Eng. Chem. Proc. Res. Dev. 11 (1972) 234.
[8] R.B. Grieves, D. Bhattacharyya, W.G. Schomp, J.L. Bewley, Membrane ultrafiltration of a nonionic surfactant, AIChE J. 19 (1973) 766.
[9] J.J.S. Shen, R.F. Probstein, On the prediction of limiting flux in laminar ultrafiltration of macromolecular solutions, Ind. Eng. Chem. Fundam. 16 (1977) 459.
[10] A.G. Fane, Ultrafiltration of suspensions, J. Membr. Sci. 20 (1984) 249.
[11] M.J. Clifton, N. Abidine, P. Aptel, V. Sanchez, Growth of the polarization layer in ultrafiltration with hollow-fiber membranes, J. Membr. Sci. 21 (1984) 233.
[12] J.G. Wijmans, S. Nakao, C.A. Smolders, Flux limitation in ultrafiltration: osmotic pressure model and gel layer model, J. Membr. Sci. 20 (1984) 115.
[13] A.A. Kozinki, E.N. Lightfoot, Protein ultrafiltration: a general example of boundary layer filtration, AIChE J. 18 (1972) 1030.
[14] W. Leung, R.F. Probstein, Low polarization in laminar ultrafiltration of macromolecular solutions, Ind. Eng. Chem. Fundam. 18 (1979) 274.
[15] R.P. Wendt, E. Klein, F.F. Holland, K.E. Eberle, Hollow fiber ultrafiltration of calf serum and albumin in the pregel uniform-wall-flux region, Chem. Eng. Commun. 8 (1981) 251.
[16] S. Nakao, S. Kimura, Model of membrane transport phenomena and their applications for ultrafiltration data, J. Chem. Eng. Jpn. 15 (1982) 200.
[17] C. Kleinstreuer, M.S. Paller, Laminear dilute suspension flows in plate-and-frame ultrafiltration units, AIChE J. 29 (1983) 529.
[18] R.P. Ma, C.H. Gooding, W.K. Alexander, A dynamic model for low-pressure, hollow-fiber ultrafiltration, AIChE J. 31 (1985) 1782.
[19] H. Nabetani, M. Nakajima, A. Watanable, S. Nakao, S. Kumura, Effects of osmotic pressure and adsorption on ultrafiltration of ovalbumin, AIChE J. 36 (1990) 907.
[20] B.H. Chiang, M. Cheryan, Ultrafiltration on skim milk in hollow fibers, J. Food Sci. 51 (1986) 340.
[21] M. Assadi, D.A. White, A model for determining the steady state flux of inorganic microfiltration membrane, Chem. Eng. J. 48 (1992) 11.
[22] H.M. Yeh, T.W. Cheng, Resistance-in-series for membrane ultrafiltration in hollow fiber of tube-and-shell arrangement, Sep. Sci. Technol. 28 (1993) 1341.
[23] J.A. Howell, Subcritical flux operation of microfiltration, J. Membr. Sci. 107 (1995) 165.
[24] D.X. Wu, J.A. Howell, R. Fired, Critical flux measurement for model colloids, J. Membr. Sci. 152 (1999) 89.
[25] L. Song, M. Elimelech, Theory of concentration polarization in crossflow filtration, J. Chem. Soc., Faraday Trans. 91 (1995) 3389.
[26] L. Song, A new model for the calculation of the limiting flux in ultrafiltration, J. Membr. Sci. 144 (1998) 173.
[27] R.B. Bird, W.E. Stewart, E.N. Lightfoot, Transport Phenomena, Wiley, New York, 1971, pp. 42–51.
[28] H.M. Yeh, H.H. Wu, Membrane ultrafiltration in combined hollow-fiber module systems, J. Membr. Sci. 124 (1997) 93.
[29] H.M. Yeh, T.W. Cheng, Y.J. Yeh, Sizing agent recovery by membrane ultrafiltration in hollow-fiber modules, Chem. Eng. Commun. 177 (2000) 204.
[30] H.M. Yeh, J.W. Tsai, Membrane ultrafiltration in multipass hollow-fiber modules, J. Membr. Sci. 142 (1998) 61.
[31] T.W. Cheng, A study on the hollow-fiber membrane ultrafiltration, Ph.D. Thesis, National Taiwan University, Taipei, Taiwan, 1992.
[32] Y.J. Yeh, Analysis of permeate flux of membrane ultrafiltration in hollow-fiber modules, M.S. Thesis, Tamkang University, Tamsui, Taipei, Taiwan, 1995.